

## Electronic Supporting Information

### Promotion of antiferromagnetic exchange interaction of in multinuclear copper(II) complexes via fused oxamato/oxamidato ligands†

Saddam Weheabby,<sup>a</sup> Mohammad A. Abdulmalic,<sup>a</sup> Matteo Atzori,<sup>b</sup> Roberta Sessoli,<sup>b</sup> Azar Aliabadi,<sup>c</sup> and Tobias Rüffer<sup>\*a</sup>

<sup>a</sup> Technische Universität Chemnitz, Faculty of Natural Sciences, Institute of Chemistry, Inorganic Chemistry, 09107 Chemnitz, Germany.

<sup>b</sup> Dipartimento di Chimica ‘Ugo Schiff’ Università degli Studi di Firenze & INSTM RU of Firenze, Via della Lastruccia 3, 50019 Sesto Fiorentino, Italy.

<sup>c</sup> Leibniz Institute for Solid State and Materials Research IFW Dresden, Helmholtzstraße 20, 01069 Dresden, Germany.

*Dedicated to Prof. D. R. T. Zahn on the occasion of his 60th birthday.*

\* Corresponding author. E-mail address: [tobias.rueffler@chemie.tu-chemnitz.de](mailto:tobias.rueffler@chemie.tu-chemnitz.de)

## Contents

Figure S1a	IR spectrum of <b>2</b>	P3
Figure S1b	ESI-MS spectrum of <b>2</b>	P3
Figure S2	$^1\text{H}$ and $^{13}\text{C}\{^1\text{H}\}$ NMR spectra of <b>2</b>	P4
Figure S3a	IR spectrum of <b>3</b>	P5
Figure S3b	ESI-MS spectrum of <b>3</b>	P5
Figure S4	$^1\text{H}$ and $^{13}\text{C}\{^1\text{H}\}$ NMR spectra of <b>3</b>	P6
Figure S5a	IR spectrum of <b>4</b>	P7
Figure S5b	ESI-MS spectrum of <b>4</b>	P7
Figure S6	$^1\text{H}$ and $^{13}\text{C}\{^1\text{H}\}$ NMR spectra of <b>4</b>	P8
Figure S7	IR spectrum of <b>5</b>	P9
Figure S8	IR spectrum of <b>6</b>	P9
Figure S9	IR spectrum of <b>7</b>	P10
Figure S10	IR spectrum of <b>8</b>	P10
Figure S11	IR spectrum of <b>9</b>	P11
Figure S12	IR spectrum of <b>11</b>	
P11		
Figure S13	IR spectrum of <b>12</b>	P12
Figure S14	IR spectrum of <b>13</b>	P12
Table S1	Crystal and structural refinement data of <b>5'</b> – <b>8'</b>	P13
Table S2	Crystal and structural refinement data of <b>11'</b> – <b>13'</b>	P14
Figure S15	Temperature dependence of $\chi_m T$ of <b>8'</b>	P15
The solid state structure of <b>8'</b>		P16
Figure S16	ORTEP diagram of one dimeric entity formed by <b>8'</b> in the solid state.	P16
Figure S17	ORTEP diagram of one dimeric entity formed by <b>8'</b> in the solid state and all further intermolecular interactions of it.	P17
Figure S18 / Table S3	UV–Vis spectra of <b>5</b> / UV–Vis data of <b>5</b>	P18
Figure S19 / Table S4	UV–Vis spectra of <b>6</b> / UV–Vis data of <b>6</b>	P19
Figure S20 / Table S5	UV–Vis spectra of <b>7</b> / UV–Vis data of <b>7</b>	P20

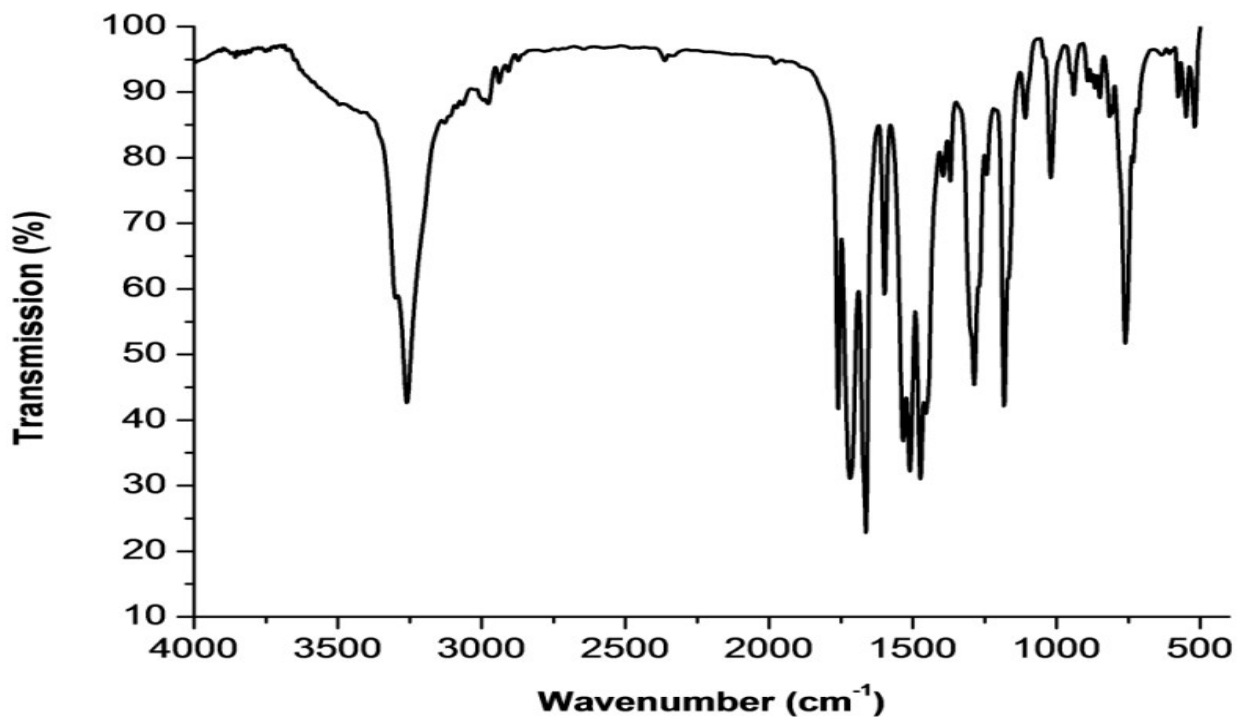


**Figure S1a.** IR spectrum (KBr) of 2.

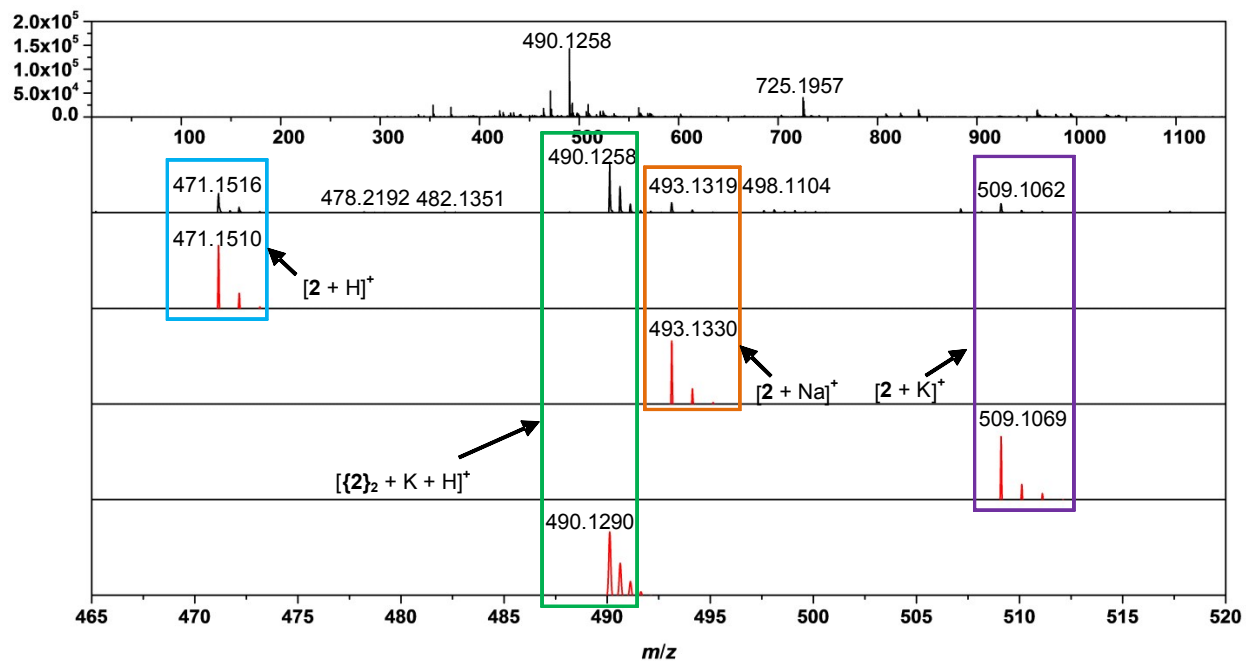


**Figure S1b.** ESI-MS spectrum of 2 (Black: Measured. Red: Calculated).

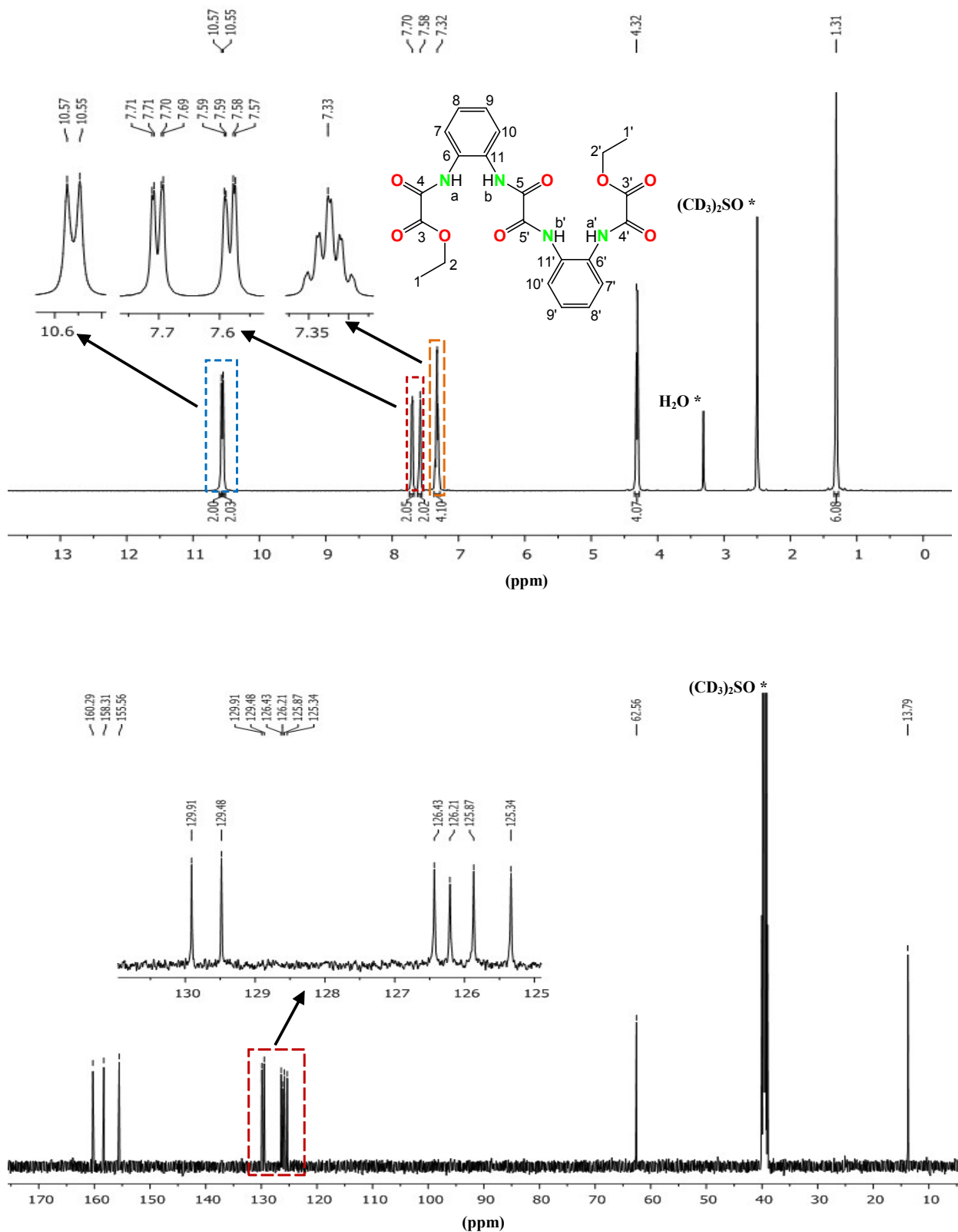


**Figure S2.**  $^1\text{H}$  (above) and  $^{13}\text{C}\{^1\text{H}\}$  NMR spectra (below) of **2**.

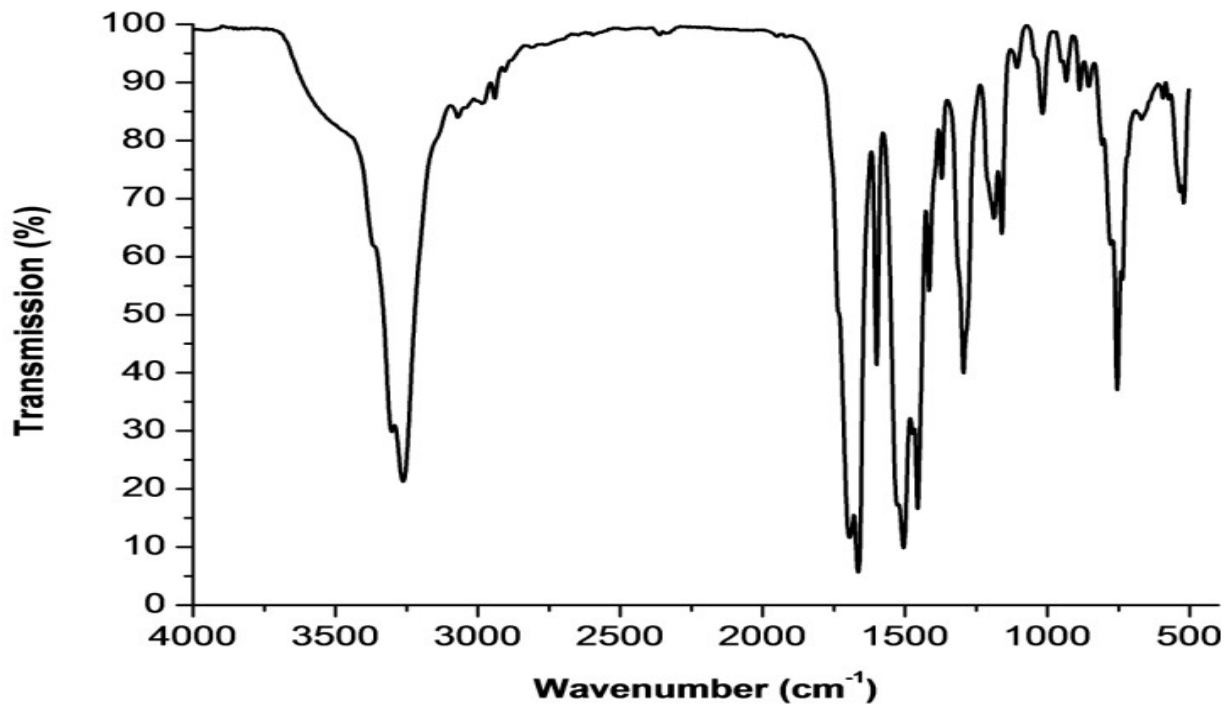


Figure S3a. IR spectrum (KBr) of 3.

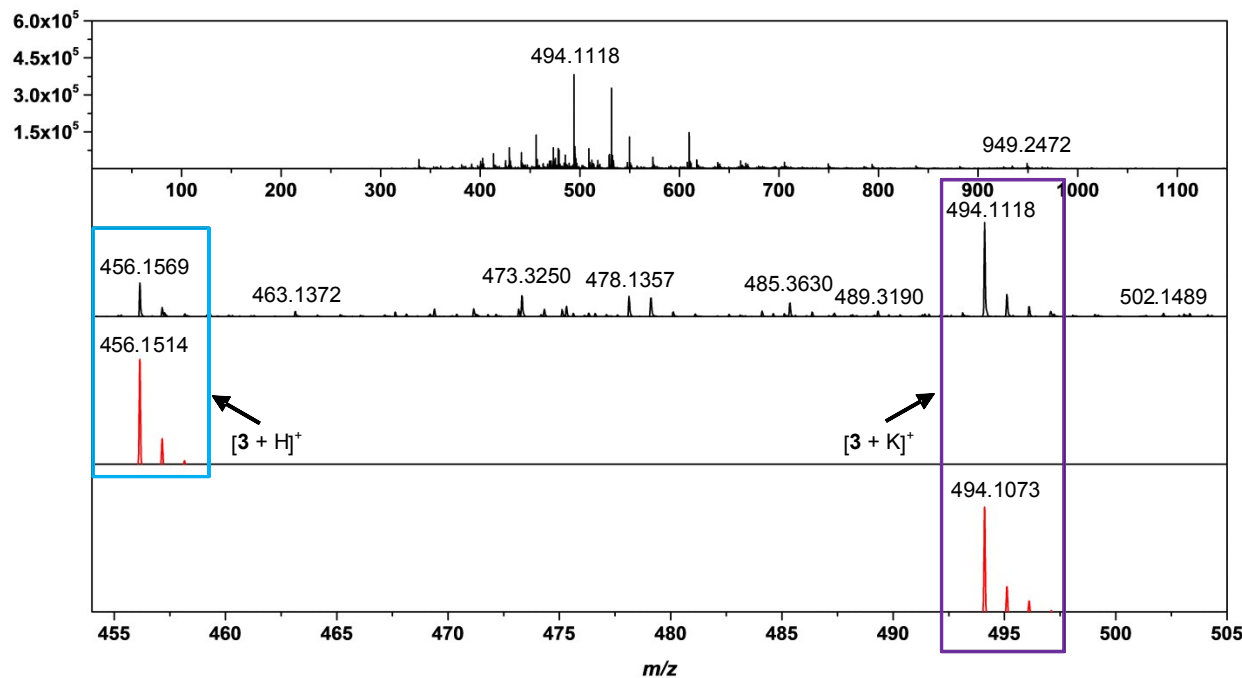
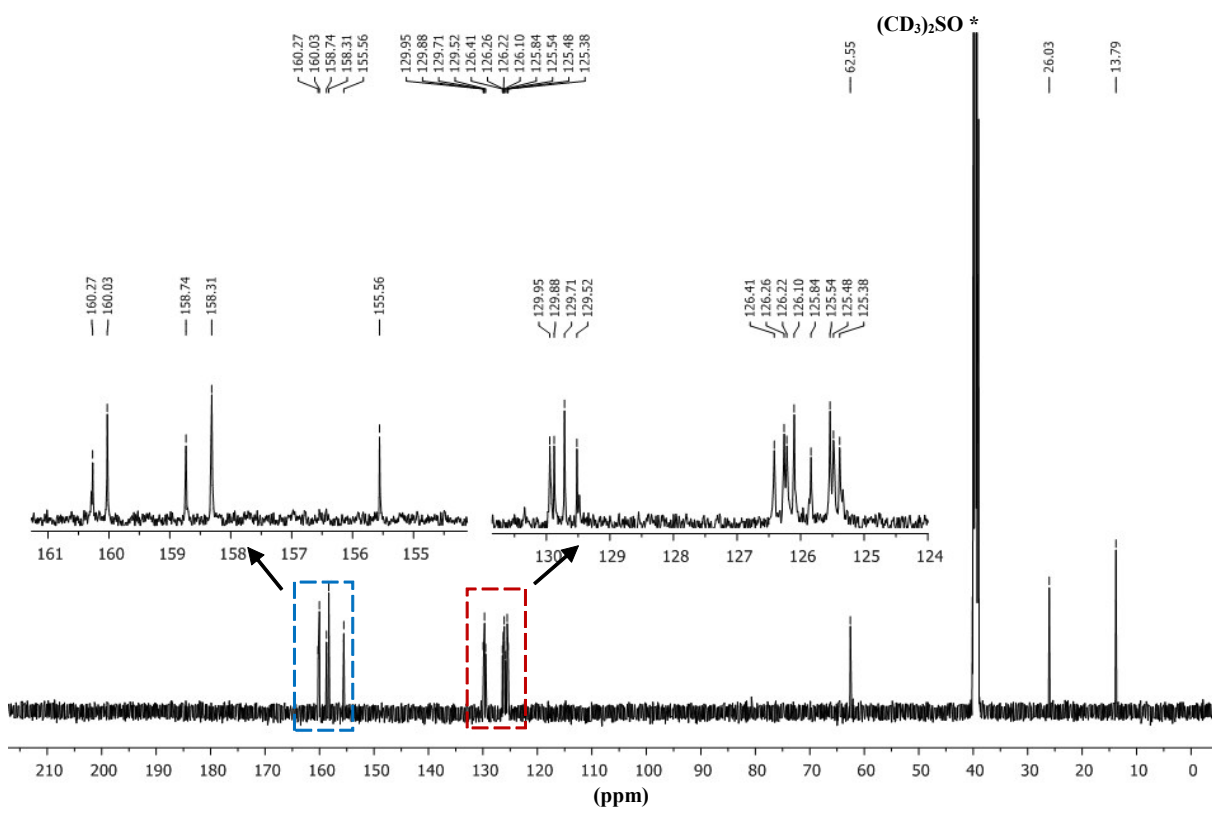
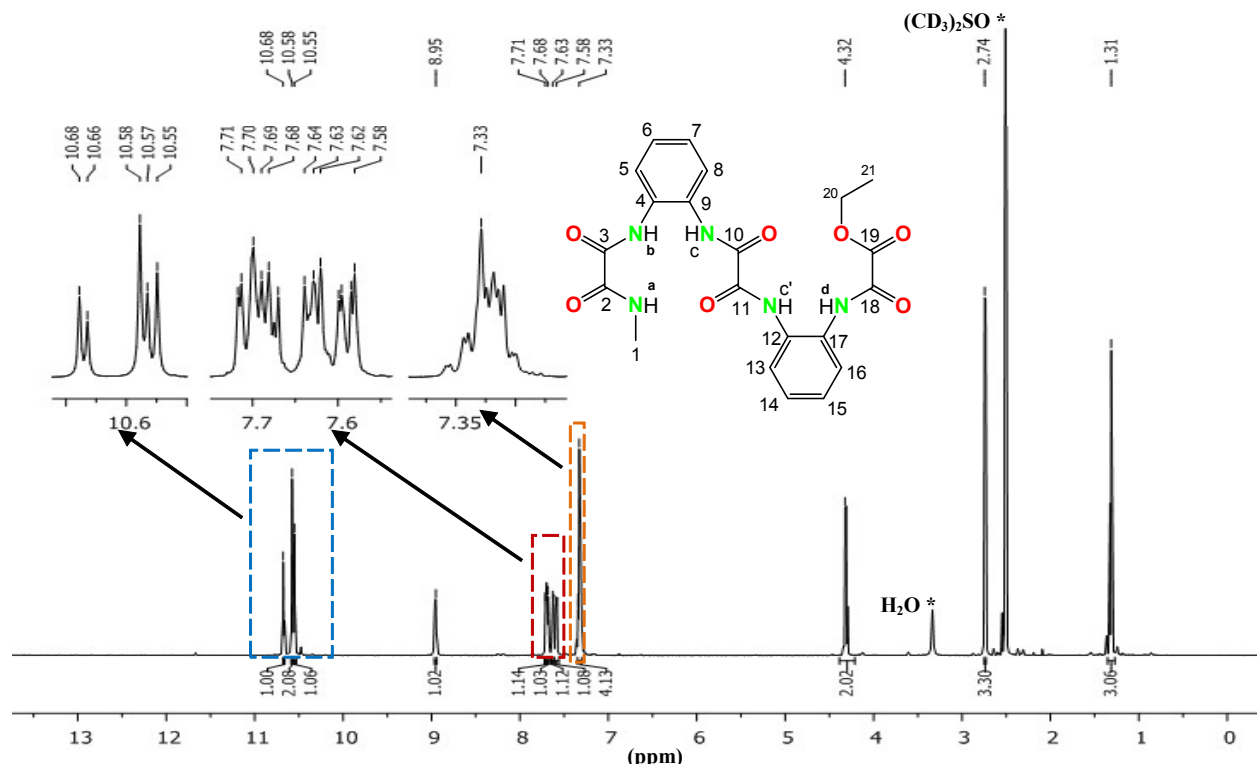


Figure S3b. ESI-MS spectrum of 3 (Black: Measured. Red: Calculated).



**Figure S4.**  $^1\text{H}$  (above) and  $^{13}\text{C}\{^1\text{H}\}$  NMR spectra (below) of **3**.

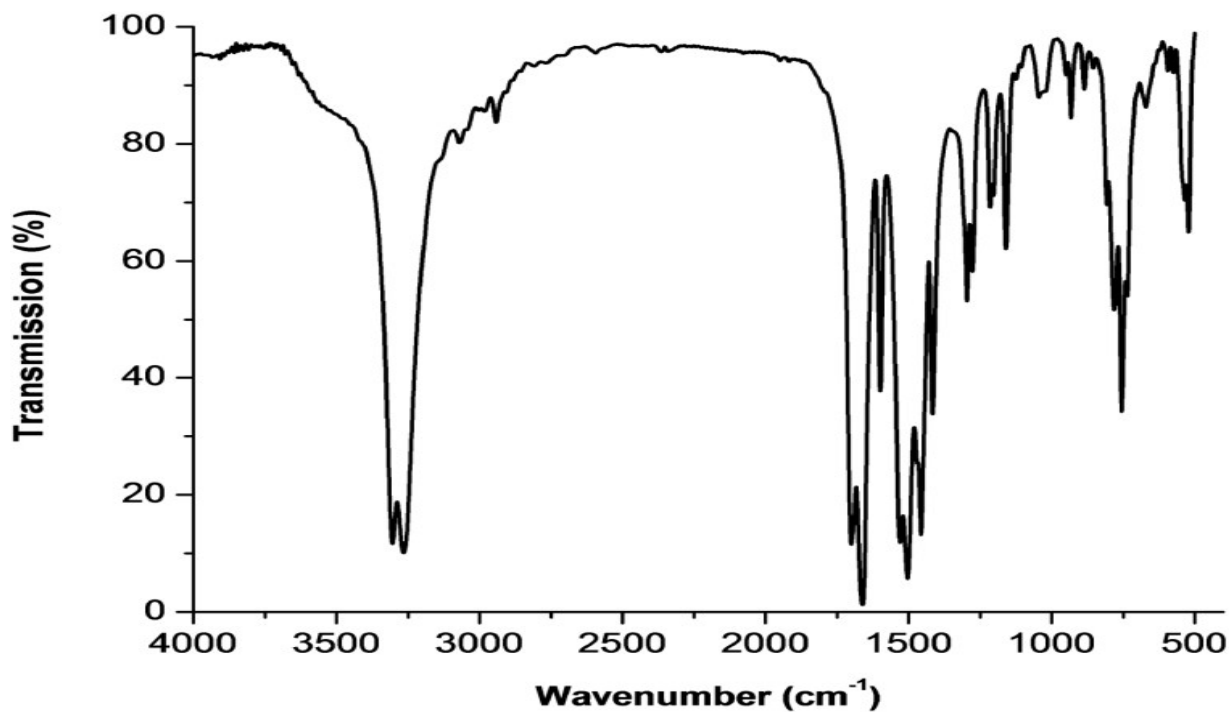


Figure S5a. IR spectrum (KBr) of 4.

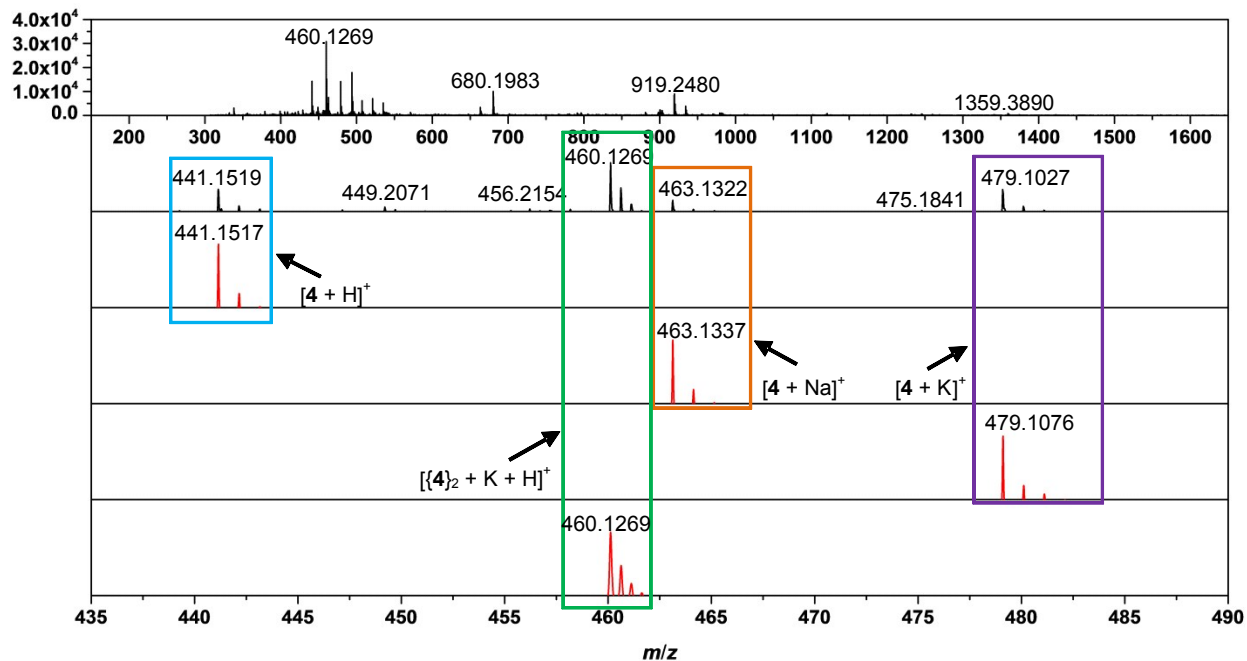
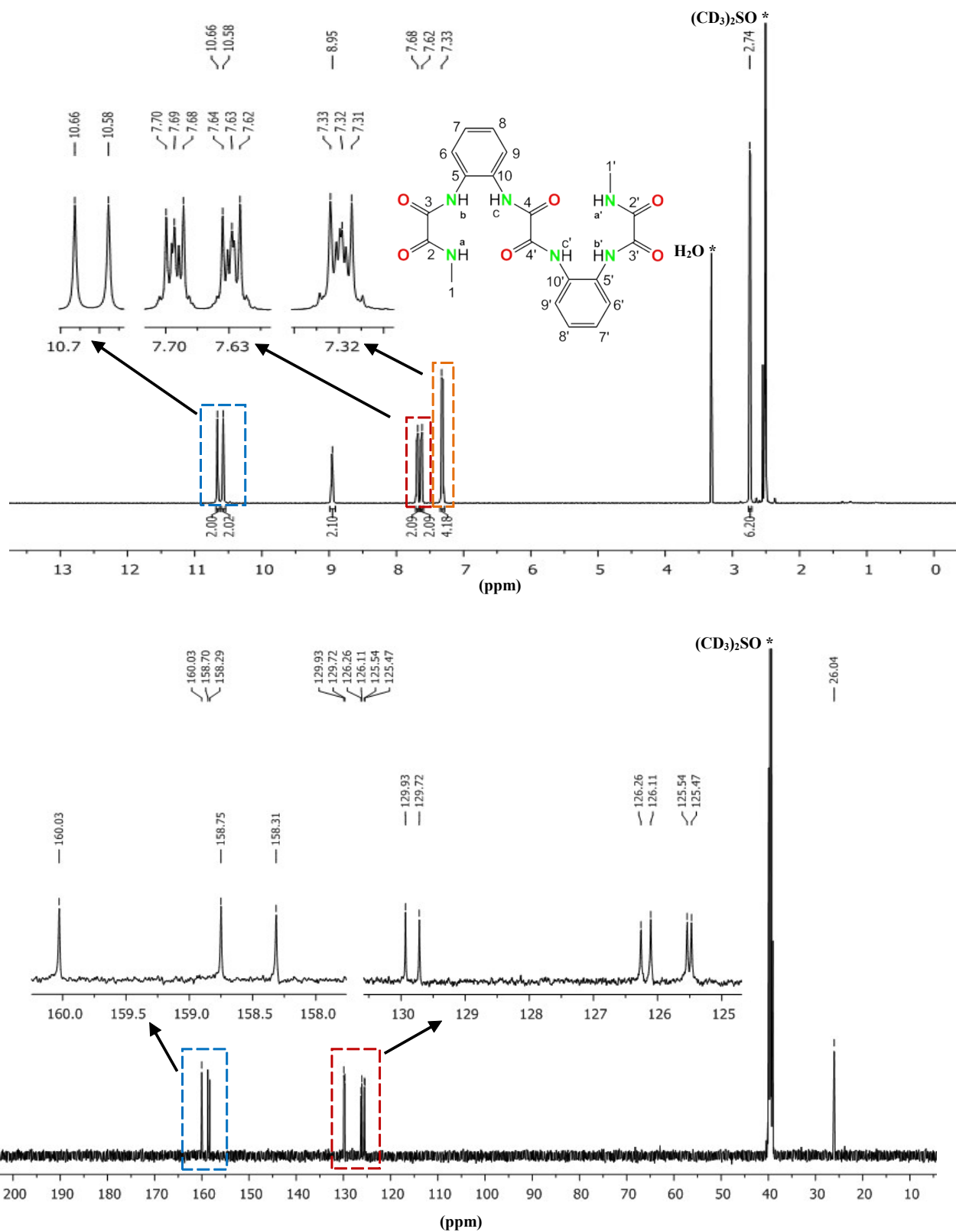
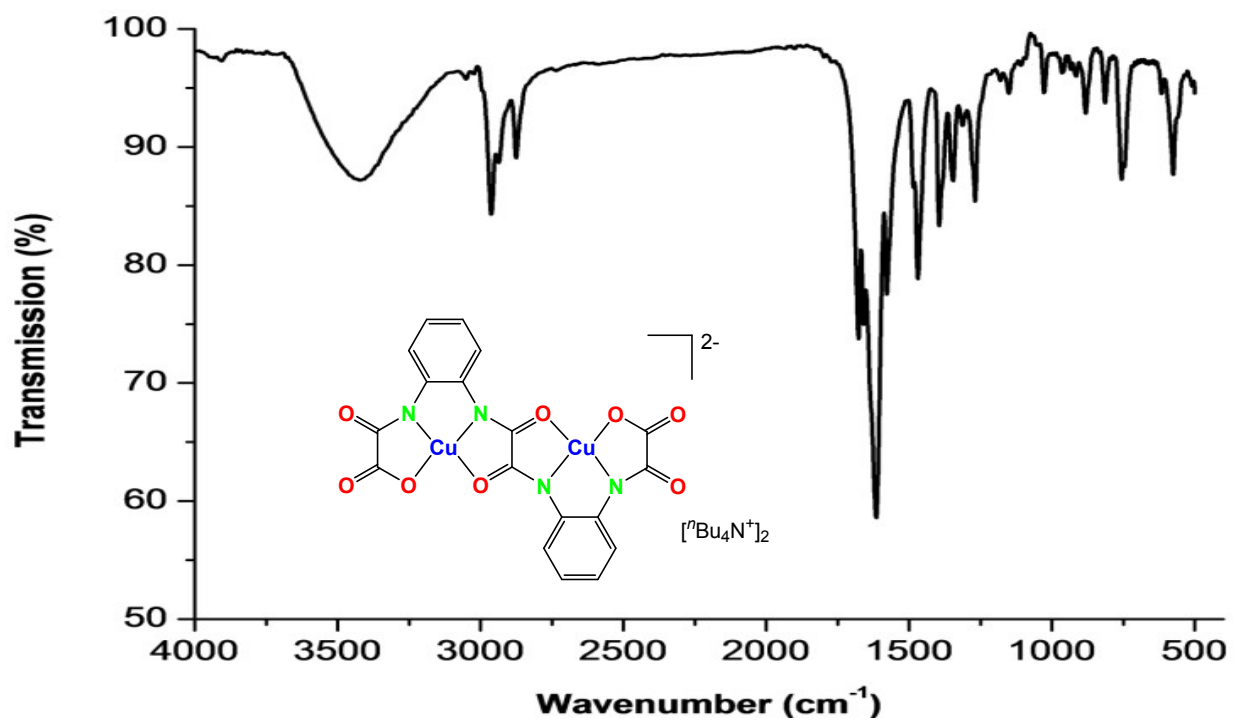


Figure S5b. ESI-MS spectrum of 4 (Black: Measured. Red: Calculated).



**Figure S6.**  $^1\text{H}$  (above) and  $^{13}\text{C}\{\text{H}\}$  NMR spectra (below) of **4**.



**Figure S7.** IR spectrum (KBr) of **5**.

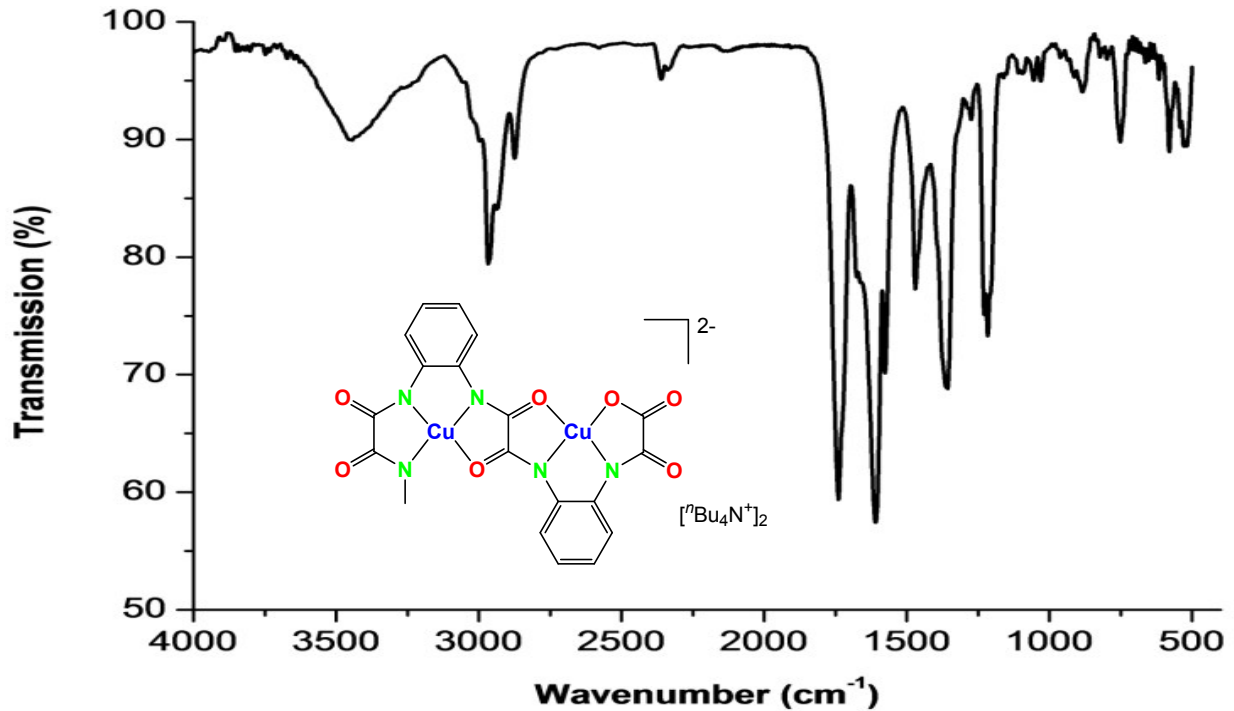


**Figure S8.** IR spectrum (KBr) of **6**.

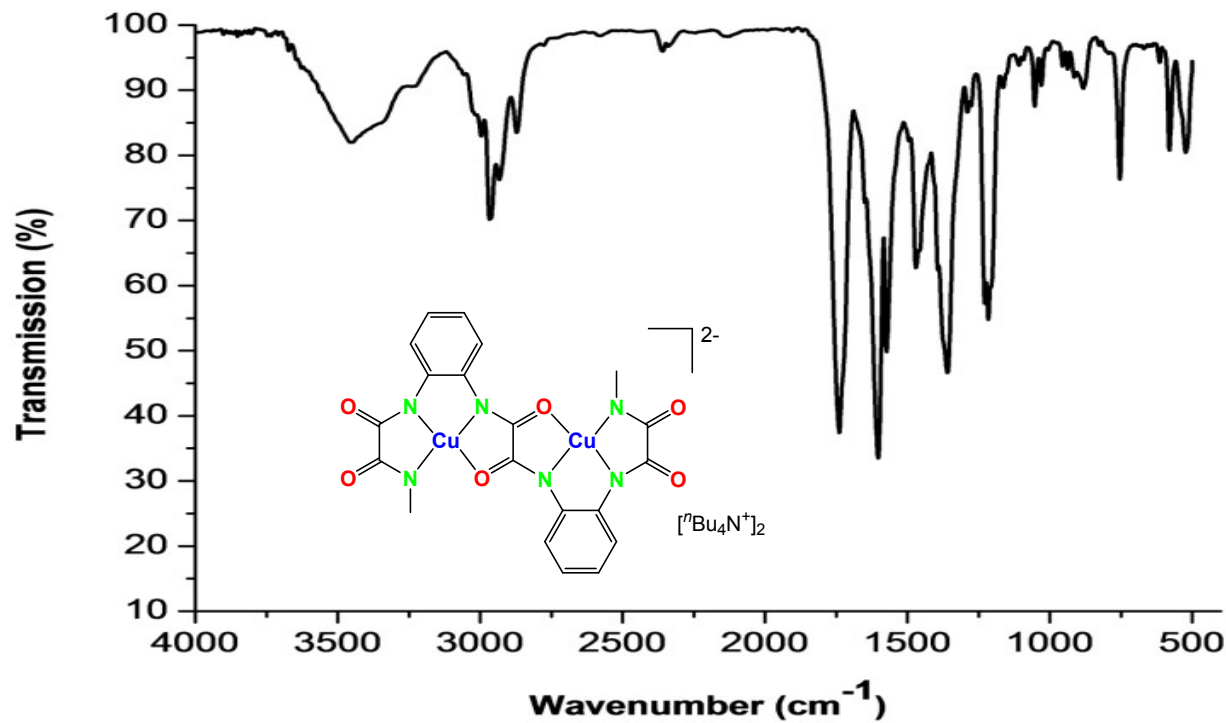


**Figure S9.** IR spectrum (KBr) of 7.

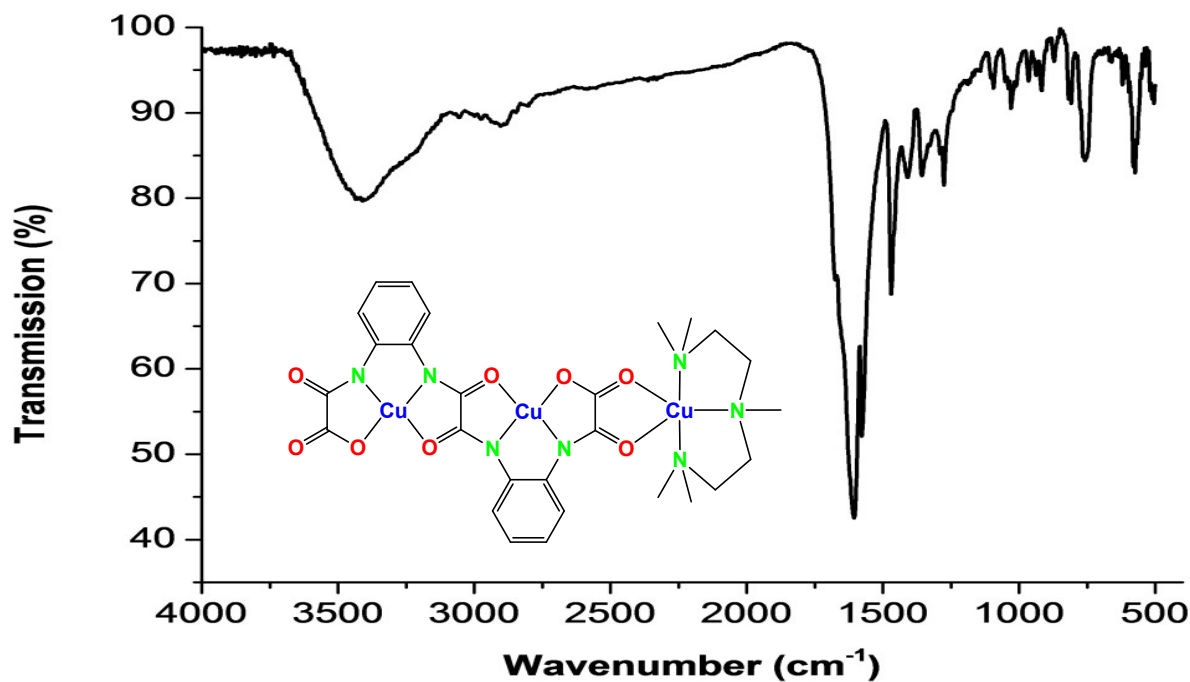


**Figure S10.** IR spectrum (KBr) of 8.

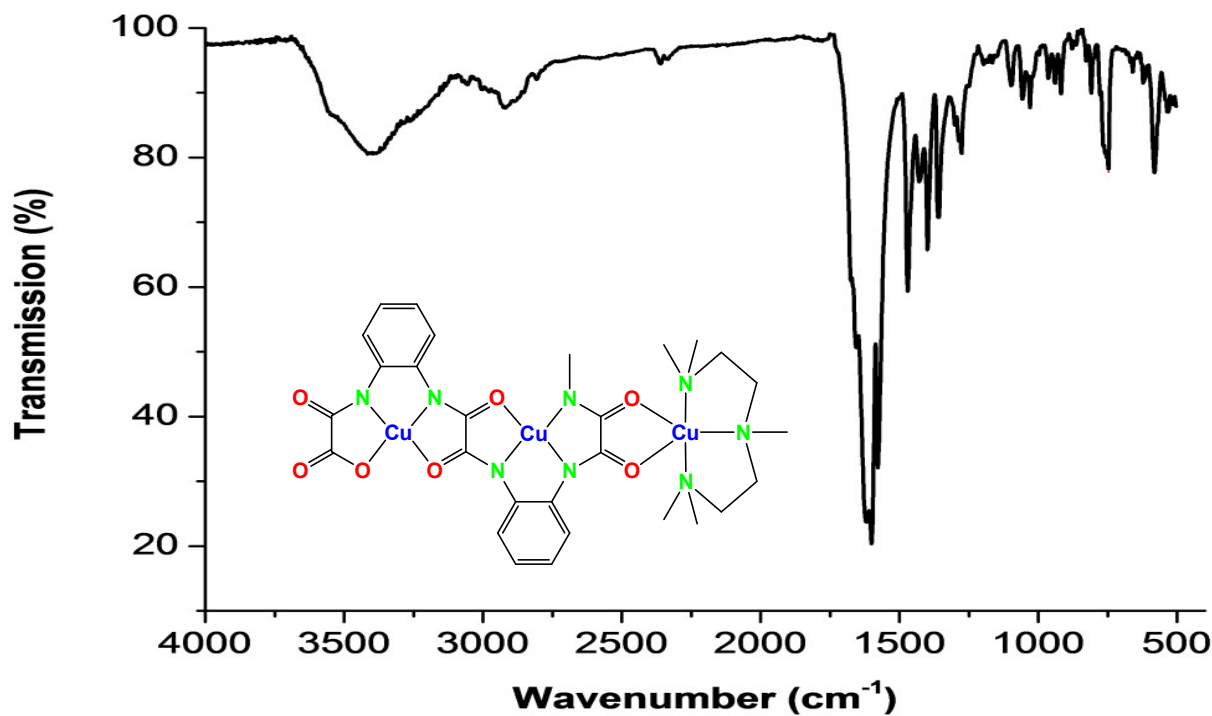


Figure S11. IR spectrum (KBr) of 9.

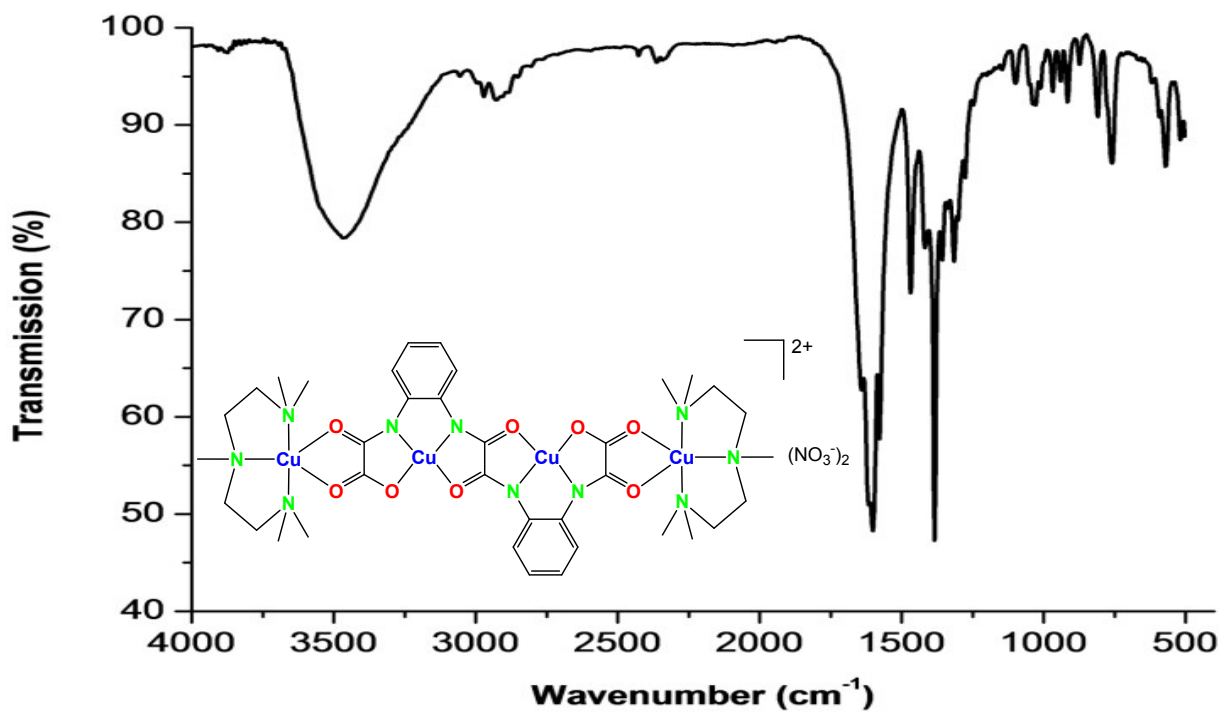


Figure S12. IR spectrum (KBr) of 11.

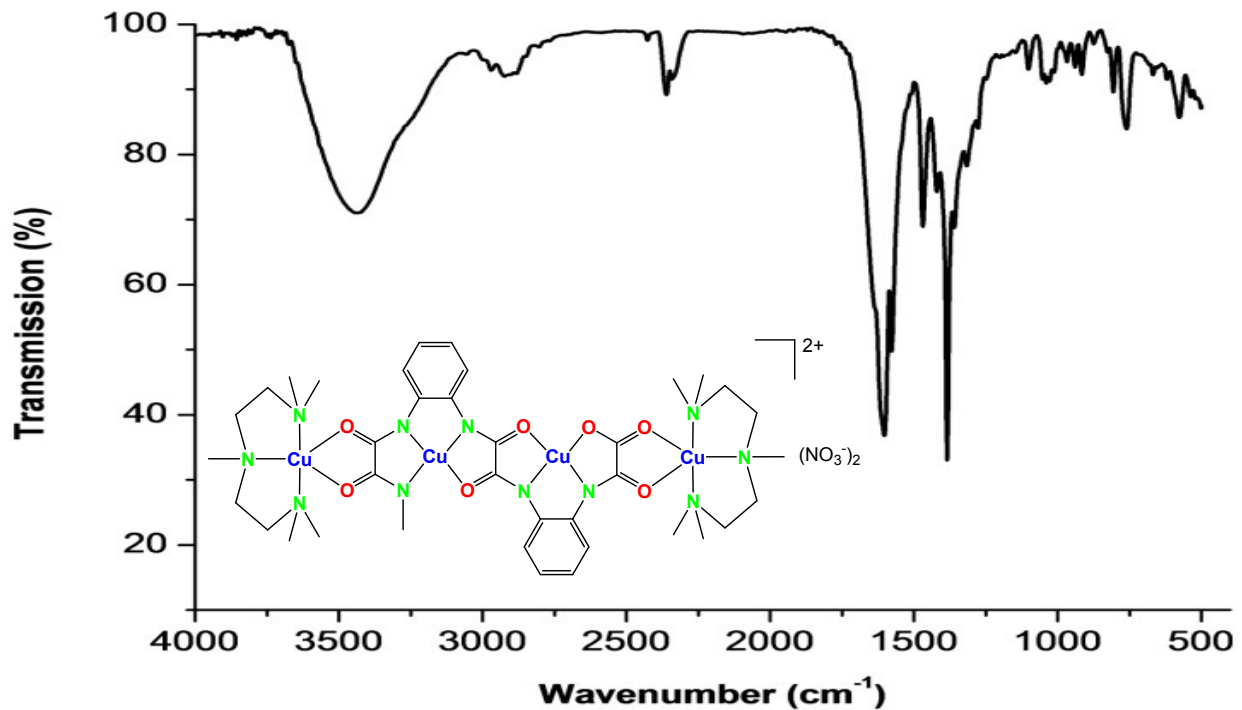


Figure S13. IR spectrum (KBr) of 12.

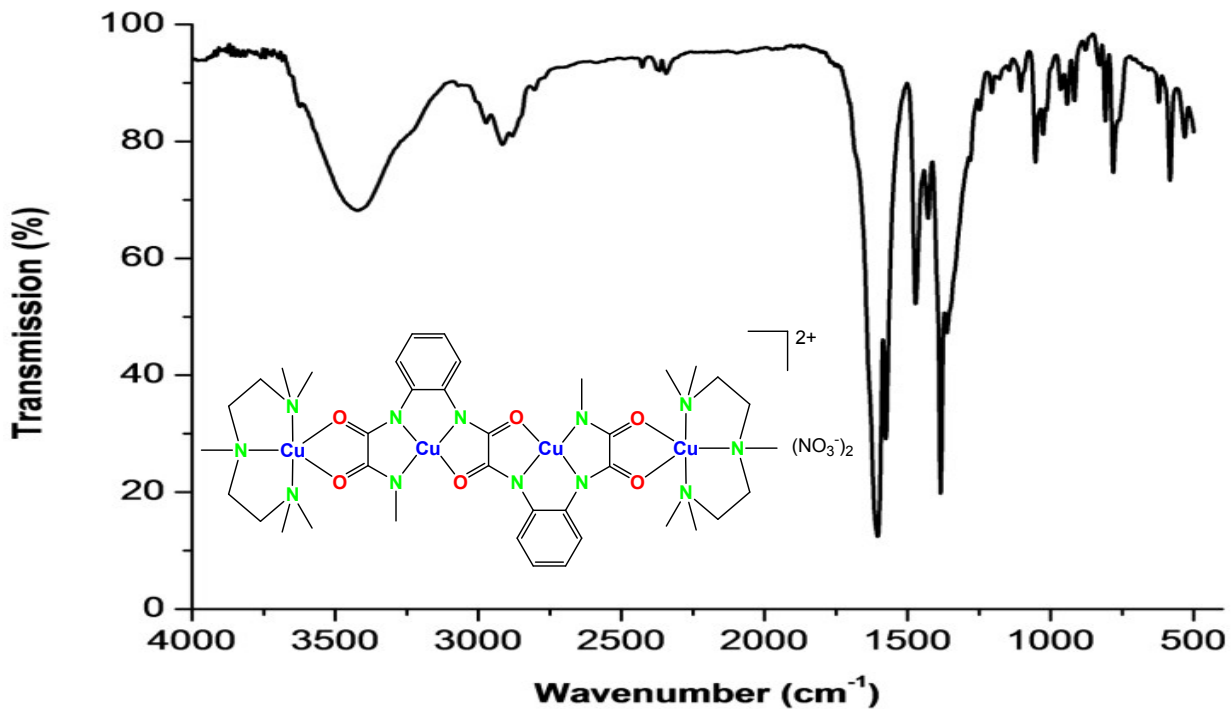


Figure S14. IR spectrum (KBr) of 13.

**Table S1.** Crystal and structural refinement data of **5'**–**8'**.

	<b>5'</b>	<b>6'</b>	<b>7'</b>	<b>8'</b>
Empirical formula	C <sub>54</sub> H <sub>96</sub> Cu <sub>2</sub> N <sub>6</sub> O <sub>12</sub>	C <sub>52</sub> H <sub>87</sub> Cu <sub>2</sub> N <sub>7</sub> O <sub>8</sub>	C <sub>52</sub> H <sub>86</sub> Cu <sub>2</sub> N <sub>8</sub> O <sub>6</sub>	C <sub>28</sub> H <sub>35</sub> Cu <sub>3</sub> N <sub>7</sub> O <sub>9</sub>
Formula mass (g·mol <sup>-1</sup> )	1148.44	1065.36	1046.36	804.25
Crystal system	monoclinic	monoclinic	monoclinic	monoclinic
Space group	P2 <sub>1</sub> /c	P2 <sub>1</sub> /c	P2 <sub>1</sub> /c	P2 <sub>1</sub> /c
<i>a</i> (Å)	10.9146(4)	11.0508(3)	15.1842(4)	12.5142(4)
<i>b</i> (Å)	17.6184(5)	17.5032(5)	17.1284(4)	14.8174(4)
<i>c</i> (Å)	15.8629(6)	15.5860(5)	22.2597(6)	17.5522(8)
$\alpha$ (°)	90	90	90	90
$\beta$ (°)	105.614(4)	108.782(3)	109.748	110.656(4)
$\gamma$ (°)	90	90	90	90
<i>V</i> (Å <sup>3</sup> )	2937.83(18)	2854.18(15)	5448.8(3)	3045.4(2)
<i>Z</i>	2	2	4	4
<i>D</i> <sub>calc</sub> (Mg·m <sup>-3</sup> )	1.298	1.240	1.276	1.754
Wavelength (Å)	1.54184	1.54184	0.71073	1.54184
Temperature (K)	110	110	110	110
Absorption coefficient (mm <sup>-1</sup> )	1.399	1.353	0.834	3.007
<i>F</i> (000)	1232	1140	2240	1644
Reflection collected	9499	9177	29458	18036
Reflection unique / <i>R</i> <sub>int</sub> <sup>a)</sup>	4969 / 0.0228	5037 / 0.0196	9449 / 0.0255	5122 / 0.0358
Max. and min. transmission	1.00000 and 0.73049	1.00000 and 0.82164	1.00000 and 0.81647	1.00000 and 0.67132
Goodness-of-fit on <i>F</i> <sup>2</sup> <sup>b)</sup>	0.939	1.092	1.031	1.044
Data / restraints / parameters	4969 / 0 / 338	5037 / 288 / 348	9449 / 0 / 613	5122 / 2 / 428
$\theta$ range for data collection (°)	3.830 to 64.969	3.918 to 67.835	3.024 to 24.998	4.813 to 65.000
Limiting indices	$-4 \leq h \leq 12$ , $-20 \leq k \leq 20$ , $-18 \leq l \leq 18$	$-13 \leq h \leq 12$ , $-20 \leq k \leq 20$ , $-11 \leq l \leq 18$	$-18 \leq h \leq 18$ , $-20 \leq k \leq 19$ , $-26 \leq l \leq 26$	$-10 \leq h \leq 14$ , $-17 \leq k \leq 17$ , $-20 \leq l \leq 20$
Final <i>R</i> indices [ <i>I</i> > 2σ( <i>I</i> )] <sup>c)</sup>	<i>R</i> <sub>1</sub> = 0.0528, <i>wR</i> <sub>2</sub> = 0.1420	<i>R</i> <sub>1</sub> = 0.0813, <i>wR</i> <sub>2</sub> = 0.2402	<i>R</i> <sub>1</sub> = 0.0324, <i>wR</i> <sub>2</sub> = 0.0803	<i>R</i> <sub>1</sub> = 0.0363, <i>wR</i> <sub>2</sub> = 0.0942
<i>R</i> indices (all data) <sup>c)</sup>	<i>R</i> <sub>1</sub> = 0.0586, <i>wR</i> <sub>2</sub> = 0.1475	<i>R</i> <sub>1</sub> = 0.0922, <i>wR</i> <sub>2</sub> = 0.2543	<i>R</i> <sub>1</sub> = 0.0436, <i>wR</i> <sub>2</sub> = 0.0848	<i>R</i> <sub>1</sub> = 0.0438, <i>wR</i> <sub>2</sub> = 0.0990
Largest diff. peak/hole (e·Å <sup>-3</sup> )	0.886/−0.366	1.641/−0.925	0.360/−0.247	0.501/−0.564

<sup>a)</sup>  $R_{\text{int}} = \Sigma |F_{\text{o}}^2 - F_{\text{o}}^2(\text{mean})| / \Sigma F_{\text{o}}^2$ , where  $F_{\text{o}}^2(\text{mean})$  is the average intensity of symmetry equivalent diffractions. <sup>b)</sup>  $S = [\sum w(F_{\text{o}}^2 - F_{\text{c}}^2)^2] / (n - p)^{1/2}$ , where  $n$  = number of reflections,  $p$  = number of parameters. <sup>c)</sup>  $R = [\sum(|F_{\text{o}}| - |F_{\text{c}}|) / \sum |F_{\text{o}}|]$ ;  $wR = [(\sum(w(F_{\text{o}}^2 - F_{\text{c}}^2)^2)) / (\sum(wF_{\text{o}}^4))]^{1/2}$ .

**Table S2.** Crystal and structural refinement data for **11'**–**13'**.

	<b>11'</b>	<b>12'</b>	<b>13'</b>
Empirical formula	C <sub>40</sub> H <sub>64</sub> Cu <sub>4</sub> N <sub>12</sub> O <sub>15</sub>	C <sub>154</sub> H <sub>242</sub> Cu <sub>16</sub> N <sub>54</sub> O <sub>54</sub>	C <sub>82</sub> H <sub>138</sub> Cu <sub>8</sub> N <sub>28</sub> O <sub>27</sub>
Formula mass (g·mol <sup>-1</sup> )	1207.19	4730.64	2456.52
Crystal system	orthorhombic	monoclinic	monoclinic
Space group	<i>Pbca</i>	<i>C2/c</i>	<i>P21/c</i>
<i>a</i> (Å)	15.0218 (8)	29.0609(15)	11.1200(3)
<i>b</i> (Å)	11.1523 (5)	15.6531(8)	23.0600(8)
<i>c</i> (Å)	31.3800 (16)	12.2183(5)	21.5519(6)
$\alpha$ (°)	90	90	90
$\beta$ (°)	90	92.987(4)	92.680(3)
$\gamma$ (°)	90	90	90
<i>V</i> (Å <sup>3</sup> )	5257.0 (5)	5550.5(5)	5520.4(3)
<i>Z</i>	4	1	2
<i>D</i> <sub>calc</sub> (Mg·m <sup>-3</sup> )	1.525	1.415	1.478
Wavelength (Å)	1.54184	1.54184	1.54184
Temperature (K)	110	110	110
Absorption coefficient (mm <sup>-1</sup> )	2.447	2.293	2.329
<i>F</i> (000)	2496	2440	2548
Reflection collected	9813	15486	17283
Reflection unique / <i>R</i> <sub>int</sub> <sup>a)</sup>	4149 / 0.0373	7490 / 0.0361	9274 / 0.0381
Max. and min. transmission	1.00000 and 0.77031	1.00000 and 0.92646	1.00000 and 0.70552
Goodness-of-fit on <i>F</i> <sup>2b)</sup>	1.150	1.011	1.029
Data / restraints / parameters	4149 / 88 / 344	7490 / 8 / 345	9274 / 14 / 692
$\theta$ range for data collection (°)	4.074 to 62.486	3.045 to 65.998	4.350 to 64.999
Limiting indices	$-17 \leq h \leq 14$ , $-8 \leq k \leq 12$ , $-35 \leq l \leq 36$	$-34 \leq h \leq 34$ , $-18 \leq k \leq 18$ , $-14 \leq l \leq 12$	$-13 \leq h \leq 10$ , $-12 \leq k \leq 27$ , $-22 \leq l \leq 25$
Final <i>R</i> indices [ <i>I</i> > 2σ( <i>I</i> )] <sup>c)</sup>	<i>R</i> <sub><i>I</i></sub> = 0.0618, <i>wR</i> <sub><i>I</i></sub> = 0.1362	<i>R</i> <sub><i>I</i></sub> = 0.0630, <i>wR</i> <sub><i>I</i></sub> = 0.1712	<i>R</i> <sub><i>I</i></sub> = 0.0543, <i>wR</i> <sub><i>I</i></sub> = 0.1477
<i>R</i> indices (all data) <sup>c)</sup>	<i>R</i> <sub><i>I</i></sub> = 0.0764, <i>wR</i> <sub><i>I</i></sub> = 0.1418	<i>R</i> <sub><i>I</i></sub> = 0.0723, <i>wR</i> <sub><i>I</i></sub> = 0.1776	<i>R</i> <sub><i>I</i></sub> = 0.0686, <i>wR</i> <sub><i>I</i></sub> = 0.1596
Largest diff. peak/hole (e·Å <sup>-3</sup> )	0.784/-0.365	0.920/-0.478	1.207/-0.718

<sup>a)</sup>  $R_{\text{int}} = \sum |F_o^2 - F_c^2(\text{mean})| / \sum F_o^2$ , where  $F_o^2(\text{mean})$  is the average intensity of symmetry equivalent diffractions. <sup>b)</sup>  $S = [\sum w(F_o^2 - F_c^2)^2]/[(n-p)^{1/2}]$ , where  $n$  = number of reflections,  $p$  = number of parameters. <sup>c)</sup>  $R = [\sum(|F_o| - |F_c|)/\sum|F_o|]$ ;  $wR = [\sum(w(F_o^2 - F_c^2)^2)/\sum(wF_o^4)]^{1/2}$ .

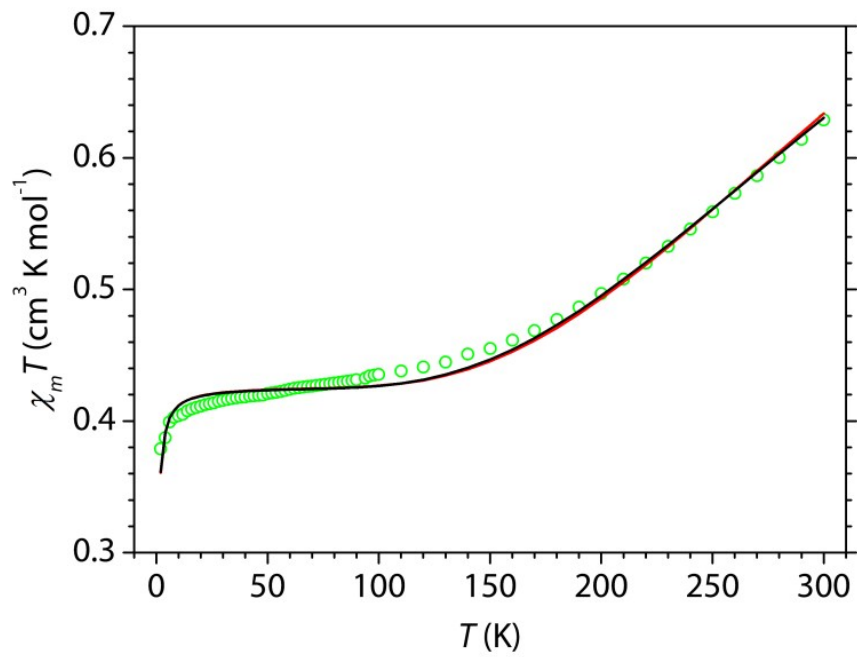


**Figure S15.** Temperature dependence of  $\chi_m T$  in the 2.0–300 K range for a polycrystalline sample of **8'** (green circles). The solid red and black lines are the best-fits of the  $\mathbf{H} = JS_A S_B - J'(\text{fixed})S_A S_C$  and  $\mathbf{H} = J(S_A S_B + S_A S_C)$  models (see text), respectively.

### The crystal structure of **8'**.

As described in the manuscript, **8'** forms a 3D network in the solid state. Central feature is the formation of dimeric entities, of which an illustration is given below in Figure S16.

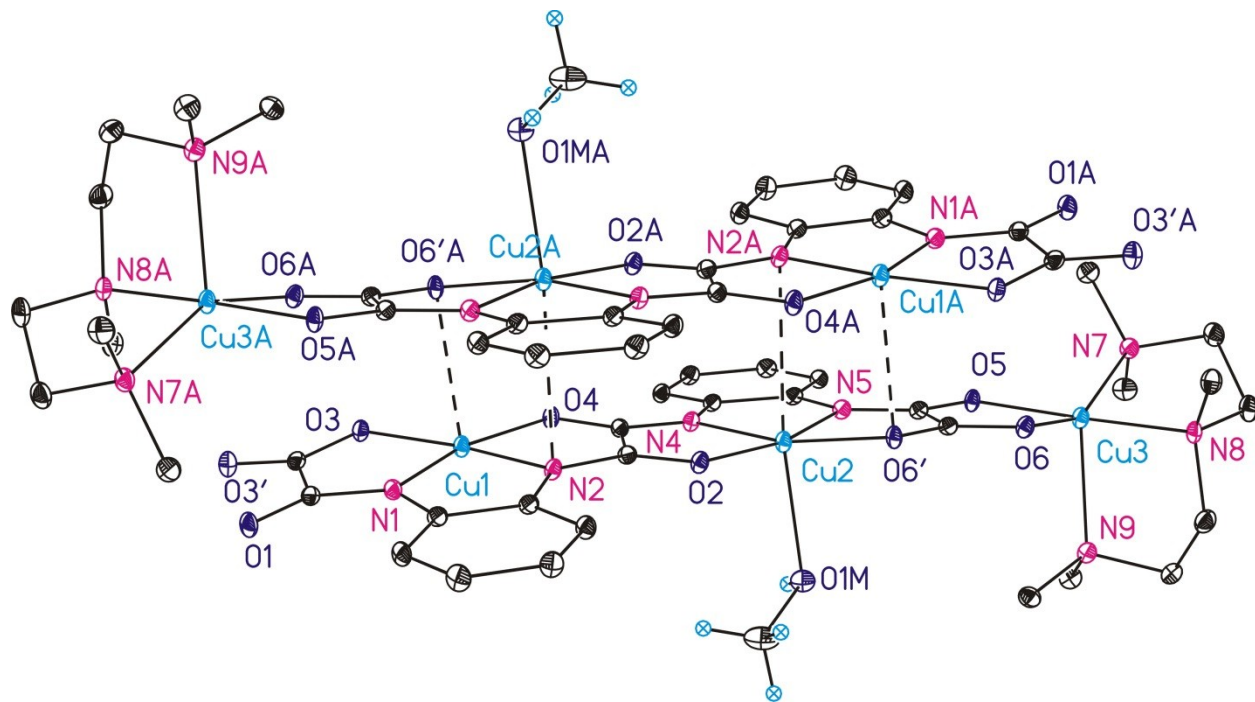


**Figure S16.** ORTEP diagram (30 % probability ellipsoids) of one dimeric entity formed by **8'** in the solid state. Beside the hydrogen atoms of the coordinating MeOH molecules all further hydrogen atoms are omitted for clarity. Dotted lines indicate the shortest inter-dimer distances with  $d(\text{Cu}1 \cdots \text{O}6'\text{A}) = 2.930 \text{ \AA}$  and  $d(\text{Cu}2\text{A} \cdots \text{N}2) = 3.224 \text{ \AA}$ .

Likely, the observed  $\text{Cu} \cdots \text{O}$  contact of the dimer is responsible for the further small intermolecular antiferromagnetic coupling of **8'** ( $J = -0.36(3) \text{ cm}^{-1}$ ), although the distance between both atoms is slightly larger compared to the sum of the van-der-Waals radii (2.930  $\text{\AA}$  versus 2.92  $\text{\AA}$ ). For comparison: For the binuclear bis(oxamato) type complex  $[\text{Cu}_2(\text{opba})(\text{pmdta})(\text{MeOH})] \cdot \frac{1}{2}\text{MeOH} \cdot \text{dmf}$  a related interaction was observed. The  $\text{Cu} \cdots \text{O}$  distance in this case amounts to 2.722  $\text{\AA}$ , although no further intermolecular magnetic exchange interaction was observed, cf. Reference S1. On the other hand, a related interaction was observed for the mononuclear  $[\text{Cu}(\text{opba})]^{2+}$  fragments, giving rise to a small inter-molecular antiferromagnetic coupling of  $J = -0.8 \text{ cm}^{-1}$ , cf. Reference S2.

As displayed in Figure S17 below, each dimeric entity of **8'** interacts in the solid state with four further dimers, of which only one is displayed. These interactions include hydrogen bond formation between the OH hydrogen donor of the coordination MeOH molecule and the O1 acceptor atom of a further molecule of **8'** ( $O1M-H1\cdots O1C$ ;  $d(D\cdots A) = 2.782(3)$  Å;  $\angle D-H\cdots A = 160(3)$ ) as well as dispersion interactions between selected aromatic subunits.

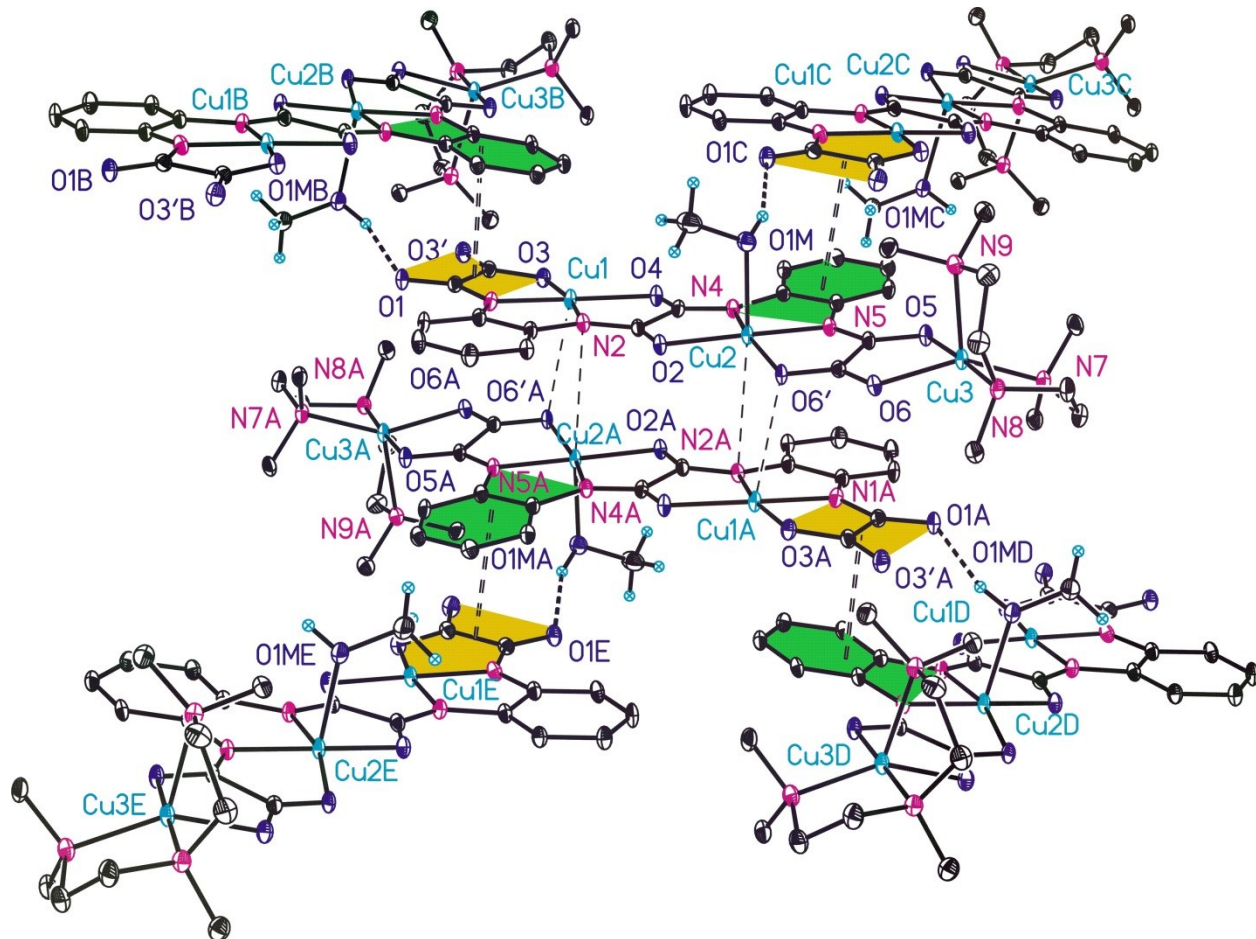


**Figure S17.** ORTEP diagram (30 % probability ellipsoids) of one dimeric entity formed by **8'** in the solid state and all further intermolecular interactions of it. Beside the hydrogen atoms of the coordinating MeOH molecules all further hydrogen atoms are omitted for clarity. Dotted lines between coloured fragments connects the geometrical centroids of atoms adjoining coloured areas ( $d = 3.38$  Å) and are used to indicate the dispersion interactions between them. Dotted indicate furthermore inter-dimer distances as well as hydrogen bond interactions.

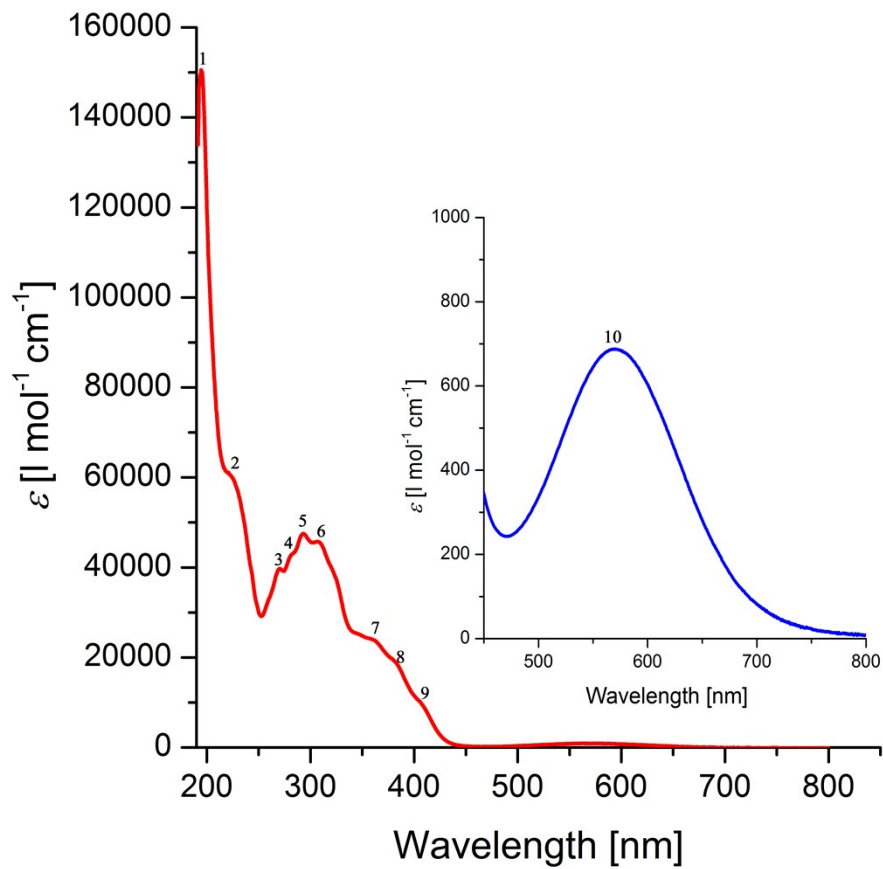


**Figure S18.** UV–Vis spectra of **5** in MeCN .

**Table S3.** UV–Vis data ( $\lambda_{\text{max}}$  [nm],  $\varepsilon$  [ $1 \text{ mol}^{-1} \text{ cm}^{-1}$ ]) of **5** at different concentrations

	Absorption $\lambda_{\text{max}}$ [nm] ( $\varepsilon$ [ $1 \text{ mol}^{-1} \text{ cm}^{-1}$ ])									
	1	2	3	4	5	6	7	8	9	10
<b>C<sub>1</sub>=9.703×10<sup>-6</sup> mol/L</b>	194.5 (150551)	221 (61104)	270 (39719)	280.5 (42512)	293 (47531)	307.5 (45738)	362 (23755)	380 (19447)	404 (10532)	—
<b>C<sub>2</sub>=4.998×10<sup>-4</sup> mol/L</b>	—	—	—	—	—	—	—	—	—	570.5 (687)

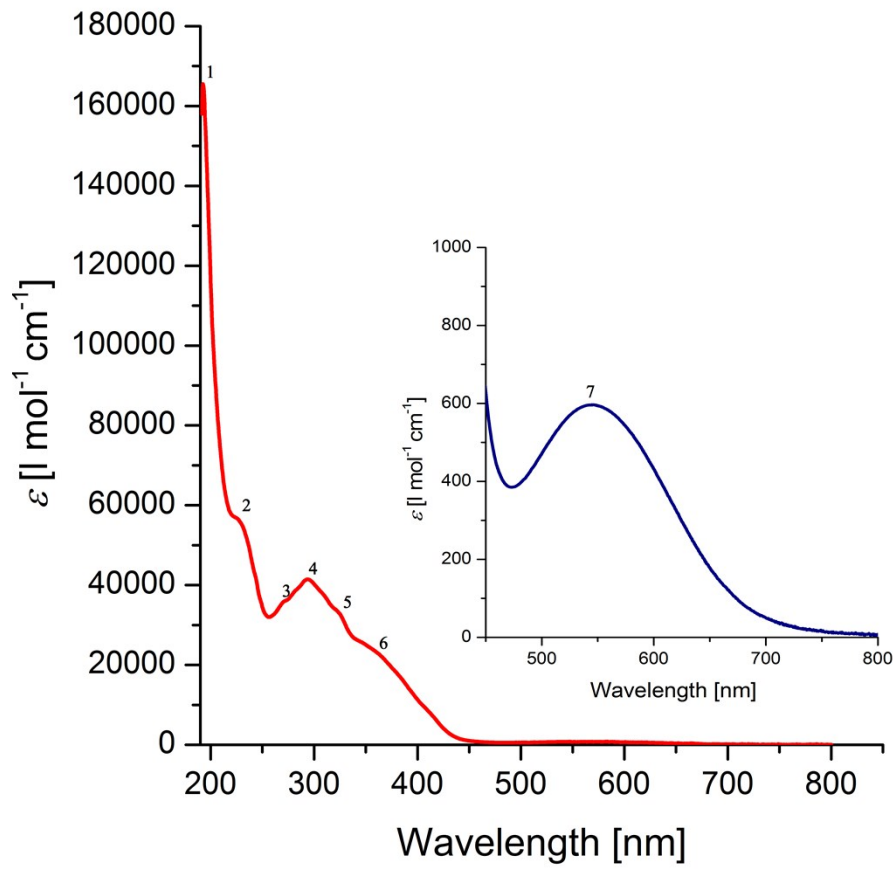


**Figure S19.** UV–Vis spectra of **6** in MeCN.

**Table S4.** UV–Vis data ( $\lambda_{\text{max}}$  [nm],  $\varepsilon$  [ $\text{l mol}^{-1} \text{cm}^{-1}$ ]) of **6** at different concentrations

	Absorption $\lambda_{\text{max}}$ [nm] ( $\varepsilon$ [ $\text{l mol}^{-1} \text{cm}^{-1}$ ])						
	<b>1</b>	<b>2</b>	<b>3</b>	<b>4</b>	<b>5</b>	<b>6</b>	<b>7</b>
<b>C<sub>1</sub>=9.703×10<sup>-6</sup> mol/L</b>	192.5 (165516)	227 (56354)	270 (35721)	293 (41440)	327 (31877)	360 (23292)	—
<b>C<sub>2</sub>=4.998×10<sup>-4</sup> mol/L</b>	—	—	—	—	—	—	545 (596)

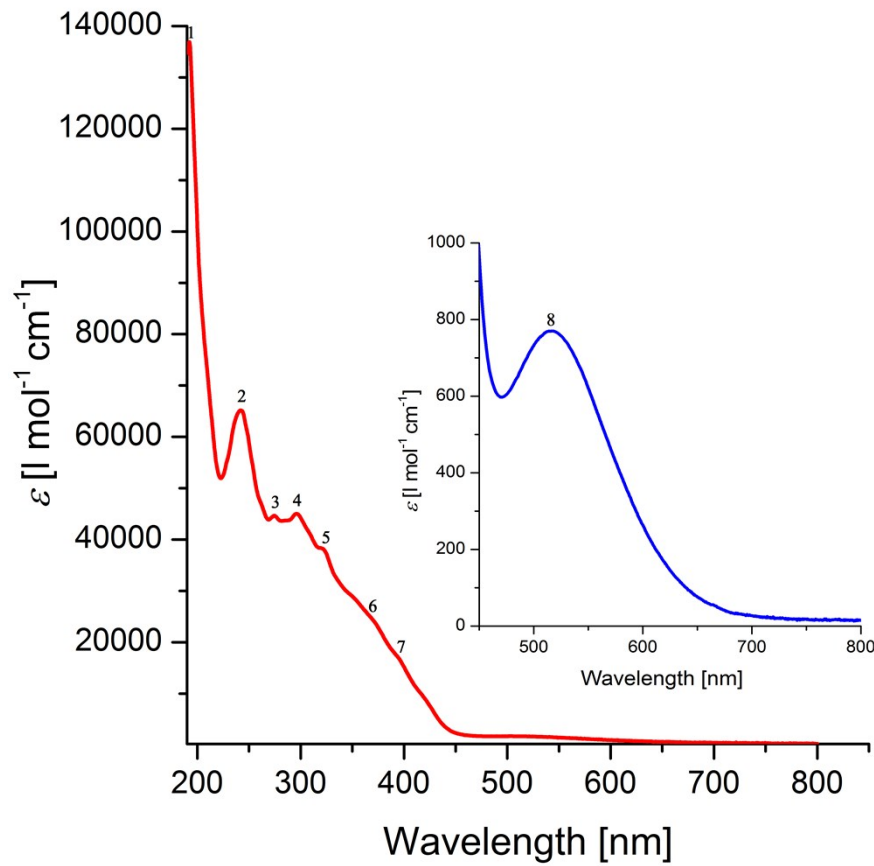


**Figure S20.** UV–Vis spectra of **7** in MeCN.

**Table S5.** UV–Vis data ( $\lambda_{\text{max}}$  [nm],  $\varepsilon$  [ $1 \text{ mol}^{-1} \text{cm}^{-1}$ ]) of **7** at different concentrations

	Absorption $\lambda_{\text{max}}$ [nm] ( $\varepsilon$ [ $1 \text{ mol}^{-1} \text{cm}^{-1}$ ])							
	<b>1</b>	<b>2</b>	<b>3</b>	<b>4</b>	<b>5</b>	<b>6</b>	<b>7</b>	<b>8</b>
<b>C<sub>1</sub>= 9.703×10<sup>-6</sup> mol/L</b>	192 (136906)	242 (65165)	274.5 (44656)	296 (45037)	321.5 (38215)	350 (28939)	372.5 (23663)	–
<b>C<sub>4</sub>= 4.998×10<sup>-4</sup> mol/L</b>	–	–	–	–	–	–	–	518 (770)

## References

- S1 T. Rüffer, B. Bräuer, F. E. Meva, L. Sorace, *Inorg. Chim. Acta.*, 2009, **362**, 563–569.
- S2 I. Unamuna, J. M. Gutiérrez-Zorilla, A. Luque, P. Román, L. Lezama, R. Calvo, T. Rojo, *Inorg. Chem.*, 1998, **37**, 6452–6460.